Front. Energy 2019, 13(2): 207–220
https://doi.org/10.1007/s11708-019-0628-9

REVIEW ARTICLE

Xi CHEN, Fangming JIN

Photocatalytic reduction of carbon dioxide by titanium oxide-based semiconductors to produce fuels

Abstract To tackle the crisis of global warming, it is imperative to control and mitigate the atmospheric carbon dioxide level. Photocatalytic reduction of carbon dioxide into solar fuels furnishes a gratifying solution to utilize and reduce carbon dioxide emission and simultaneously generate renewable energy to sustain the societies. So far, titanium oxide-based semiconductors have been the most prevalently adopted catalysts in carbon dioxide photoreduction. This mini-review provides a general summary of the recent progresses in titanium oxide-catalyzed photocatalytic reduction of carbon dioxide. It first illustrates the use of structural engineering as a strategy to adjust and improve the catalytic performances. Then, it describes the introduction of one/two exogenous elements to modify the photocatalytic activity and/or selectivity. Lastly, it discusses multi-component hybrid titanium oxide composites.

Keywords photocatalysis, carbon dioxide reduction, semiconductors, titanium oxide, renewable fuels

1 Introduction

Global warming caused by the rapid and overwhelming emission of carbon dioxide (CO_2) has become a serious and imperative worldwide issue concerning all human beings [1–3]. Due to intense anthropogenic activities, especially the massive combustion of fossil fuels, the original balance of nature carbon cycle has been gravely damaged. At present, the atmospheric CO_2 level largely deviates from its reasonable values which have been maintained in the past millions of years and reaches almost the highest level of approximately 410 ppm in history [4]. Besides, new records of high concentrations are predicted in the coming years with the current increasing rate. To fight against climate change, scientists have made persistent endeavors to capture, store, and utilize CO_2 in efficient and feasible ways [5–9]. It is devised that CO_2 can be utilized as an ample, low-cost, and readily available C1 platform resource to produce diverse chemicals and fuels, including formic acid (HCOOH), methanol (CH_3OH), carbon monoxide (CO), methane (CH_4), ethane (C_2H_6), etc [10–12] (see Fig. 1(a)). The C1 chemistry based on CO_2 as a starting material puts forward a new direction to furnish the societies with energy and decrease the reliance on fossil oils, which could potentially close carbon cycle and realize zero-net carbon emission. Nevertheless, one important concern related with CO_2 refinery into fuels is the required energy input to proceed the conversion which may partially or sometimes completely offset the produced energy fuels. As a result, if the used energy is generated from non-renewable fossil fuels, the energy consumption of the reaction systems must be minimized by all kinds. However, to maximize the efficacy of producing fuels from CO_2, another option is to exploit renewable energy for the reduction of CO_2 to generate chemicals and fuels.

Solar energy represents a type of clean, sustainable, and abundant energy source. Based on estimations, the total solar energy reaching the planet per hour upon full utilization could approximately meet the demand of the annual global energy consumption [13]. Photocatalytic reduction of CO_2 using semiconductors provides a viable and promising way to harness solar energy and store it in the form of chemical fuels. It resembles the natural photosynthesis in plants transforming CO_2 and water into carbohydrates, whereas in photocatalytic reduction, rationally designed or modified semiconductors are employed as the catalysts to accelerate the reaction rates, adjust the

Received Dec. 15, 2018; accepted Feb. 21, 2019; online May 25, 2019

Xi CHEN
China-UK Low Carbon College, Shanghai Jiao Tong University, Shanghai 201306, China

Fangming JIN (✉)
China-UK Low Carbon College, Shanghai Jiao Tong University, Shanghai 201306, China; School of Environmental Science and Engineering, State Key Laboratory of Metal Matrix Composites, Shanghai Jiao Tong University, Shanghai 200240, China
E-mail: fmjin@sjtu.edu.cn

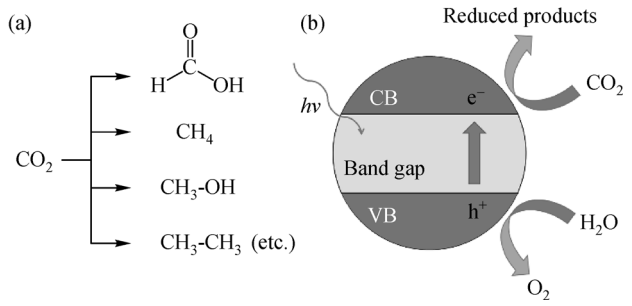

Fig. 1 Devised utilization of CO_2 as an ample, low-cost, and readily available C1 platform resource
(a) Proposal of CO_2 utilization to produce chemicals and fuels; (b) schematic illustration of photocatalytic reduction of CO_2

selectivity toward different products and boost the production yields. Titanium oxide (TiO_2)-based materials have been the most widespread semiconductors used for photocatalytic CO_2 reduction since its first application in 1979 [14], primarily because it is non-toxic, inexpensive, stable, resistant to photo-corrosion, and abundant. The principle of photocatalytic reduction of CO_2 is illustrated in Fig. 1(b). A semiconductor is characterized by its band gap structure. Above the gap lies the conduction band (CB), and below the gap lies the valence band (VB). For TiO_2 materials, the band gap is usually around approximately 3 eV, and thus untreated TiO_2 absorbs energy mainly in the ultraviolet (UV) range. Upon irradiation, an electron can be excited from the VB to the CB, which simultaneously creates an empty state referred to as a hole in the VB. The isolated electron and hole (the charge carrier) may transfer to the surface and serve as active sites to reduce or oxidize adsorbed reactants respectively. Thus, the efficient separation of the electron-hole pairs is fundamentally crucial to improve the photocatalytic efficiency.

Since UV light only accounts for less than 10% and visible light accounts for about 43% of the full spectra of solar energy, various methods have been explored to prepare visible light responsive TiO_2 materials, most of which can often lead to concurrent improvements in charge separation, CO_2 adsorption, etc. In addition, the suppression of hydrogen (H_2) evolution from water is also targeted in catalyst design to enhance the photocatalytic selectivity toward CO_2 reduction. Generally, these methods involve two major strategies: the nanostructure engineering of TiO_2 or/and the introduction of other components to modify the catalytic system. The nanostructure engineering normally focuses on altering the crystal lattice, crystal phases, the morphology, etc. The introduction of other components includes the incorporation of one or more metal/non-metal elements, and the introduced component is often called the co-catalyst. Besides, multi-component hybrid TiO_2 composites have also been broadly reported to well utilize the synergy in different constitutes. In this mini-review, it is objective to showcase the progresses in photocatalytic reduction of CO_2 using TiO_2-based semiconductors in the past years. First, nanostructure engineering of TiO_2 to improve its photocatalytic activity in related works will be illustrated. Moreover, TiO_2 modifications by incorporating one/two other metal elements will be summarized. Furthermore, TiO_2 modifications with non-metal elements as well as multi-component hybrid TiO_2 composites will also be exemplified. Prior to this review, there have been a plethora of excellent reviews [15–22] of the reduction of CO_2 into fuels and/or chemicals with a different emphasis that can be referred to if interested. Note that this mini-review mainly focuses on TiO_2 as the photocatalyst and there have also been outstanding works using other catalysts which will not be covered here [23–25].

2 Nanostructure engineering of TiO_2

2.1 Crystal lattices and phases

The types and ratios of crystal phases in TiO_2 can considerably affect its photocatalytic activity in CO_2 reduction. Compared to single phase TiO_2 (anatase, rutile or brookite), it was deduced that a mixture of different crystal phases was more advantageous in regards of photocatalytic activity due to the generation of heterojunctions that facilitates charge transfer and separation [26,27]. Kandiel et al. found that rutile TiO_2 nanorods moderately decorated with anatase TiO_2 nanoparticles (NPs) displayed a better activity than pure and overloaded rutile TiO_2 in photocatalytic decomposition of acetaldehyde [28]. Moreover, Tan et al. synthesized oxygen-rich TiO_2 NPs using a facile aqueous peroxo-titania route [29]. The oxygen-enriched synthesis environment stimulated the formation of rutile phase TiO_2 at a relatively low calcination temperature of about 300°C (The temperature commonly required is above 600°C). As a result, the as-obtained TiO_2 NPs contained both anatase and rutile crystal phases, forming a heterojunction to promote the electron-hole separation. Moreover, enriched oxygen has also led to enhanced visible light absorption. Owing to the improved charge separation and light absorption, the dual-phase TiO_2 NPs showed >10 times higher activity than pure anatase TiO_2 when the rutile composition was 17.5%. In addition, the morphology-induced crystal structure change was also disclosed to considerably influence the photocatalytic activity of TiO_2, where the synergistic effects of both morphology and crystalline change contributed. For instance, hierarchical TiO_2 nanofibers constituted by interconnected TiO_2 NPs that formed one-dimension (1D) mesoporous nanofiber were fabricated by using a combined electrospinning and sol-gel method [30]. The 1D mesoporous nanofiber morphology boasted an

improved charge transfer rate and a decreased electron-hole recombination rate, compared to the randomly aggregated TiO_2 material. Furthermore, the 1D confinement effect induced partial phase transformation from anatase to rutile, and this heterojunction further promoted the charge separation. Using the 1D TiO_2 nanofibers annealed under static argon (Ar), CO was dominantly produced at a rate of 10.2 μmol/(g·h) at a pressure of 2 bar at 50°C under UV light irradiation.

Likewise, similar observations were made for crystal lattices. Previously, the (001) facets with high-surface-energy were known to display a better activity than (101) facets, and many techniques were established to upraise the portion of (001) facets in TiO_2 crystals to enhance photocatalytic activity of TiO_2 for CO_2 reduction [31–33]. Nonetheless, the merits of proper blends of these facets were proposed recently. In 2014, Yu et al. put forward a new concept of "surface heterojunction" and emphasized the pivotal role of cooperative effects between (001) and (101) facets [34]. A series of samples with varied facet composition were prepared using hydrofluoric acid (HF) treatment, and investigated by combined experiments and density functional theory (DFT) calculations. With a suitable ratio, the presence of (101) and (001) facets formed a heterojunction similar to type II band alignment in semiconductor-based heterostructures. The heterojunction assisted in the separation of electrons and holes to (101) and (001) facets respectively, and thus resulted in longer charge carrier lifetimes and an inhibited electron-hole recombination rate. With about 0.55 (101) facets, the highest CH_4 yield was realized at 1.35 μmol/(g·h) under UV light irradiation and atmospheric pressure at room temperature. In line with the work, oxygen-deficient TiO_2 nanocrystals with coexposed (001) and (101) facets were also synthesized to exploit the combined, positive effects of mixed crystal facets and defective sites [35]. TiO_2 nanocrystals with different exposed facets were synthesized for comparison by using a hydrothermal method, whose scanning electron microscope (SEM) and high-resolution transmission electron microscopy (HRTEM) characterizations were shown in Fig. 2. The surface and bulk Ti^{3+} /oxygen vacancy defective sites were generated by sodium borohydride ($NaBH_4$) reduction, and these defects enabled the material to be visible light responsive. The developed catalyst exhibited a much higher activity than unmodified TiO_2 and TiO_2 with merely coexposed facets or merely oxygen defects. Using the synthesized catalyst, CO was formed as the major product in the photoreduction of CO_2 by water vapor, and the yields were about 11.0 and 5.0 μmol/(g·h) (The quantum yields were 0.3% and 0.1%.) respectively under UV-vis light or visible light irradiation. Based on *in situ* analysis, coexposed facets presumably rendered a favorable environment for reversible CO_2 adsorption-desorption, while the defective sites offered extra sites for CO_2 adsorption and activation.

In material sciences, the change in shape and morphology can usually alter the crystal facets at the same time. Wu et al. conducted a mechanistic study by using DFT calculations and claimed that anatase TiO_2 nanobelts with exposed (101) facets in its two main surfaces (as shown in Fig. 3) displayed superior photocatalytic activity to spherical TiO_2 NPs with the same crystal phase and comparable specific surface area [36]. One important merit of the nanobelt was that the surfaces with (101) facets were highly reactive to interact with molecular oxygen gas (O_2) and favored the formation of active superoxide radicals. The other prominent merit was its much enhanced efficiency in the separation of photogenerated electron and hole pairs. Several reasons were proposed to explain the improved charge separation: the longitudinal dimension of nanobelts led to a better charge mobility; the adsorbed O_2 on the facet acted as electron traps to separate the charge carriers; and the number of localized states near and/or in the band gap were reduced.

In addition, the strategy to achieve an integrated engineering of the multilevel structures was sometimes employed in order to further enhance the photocatalytic

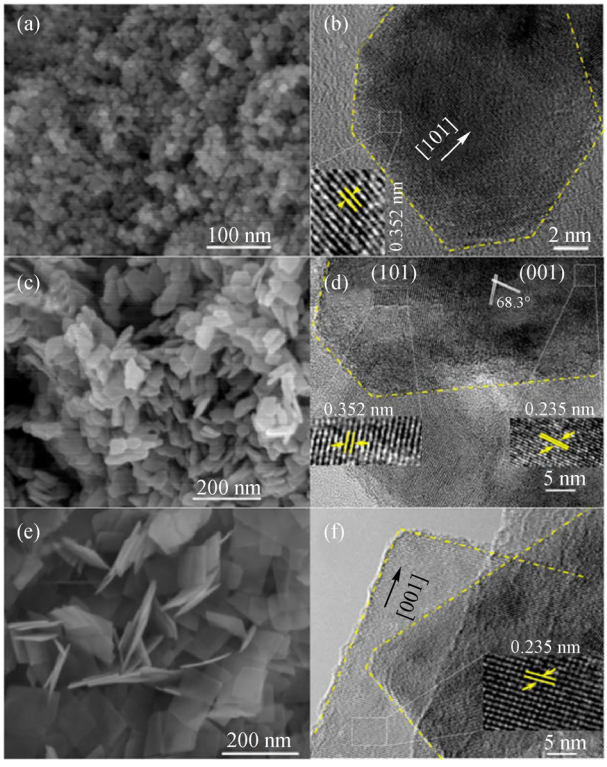

Fig. 2 SEM and HRTEM images of TiO_2 nanocrystals with different crystal facets (adapted with permission from Ref. [35]) (a) SEM image of TiO_2 with (101) facets; (b) HRTEM image of TiO_2 with (101) facets; (c) SEM image of TiO_2 with coexposed (001) and (101) facets; (d) HRTEM image of TiO_2 with coexposed (001) and (101) facets; (e) SEM image of TiO_2 with (001) facets; (f) HRTEM image of TiO_2 with (001) facets

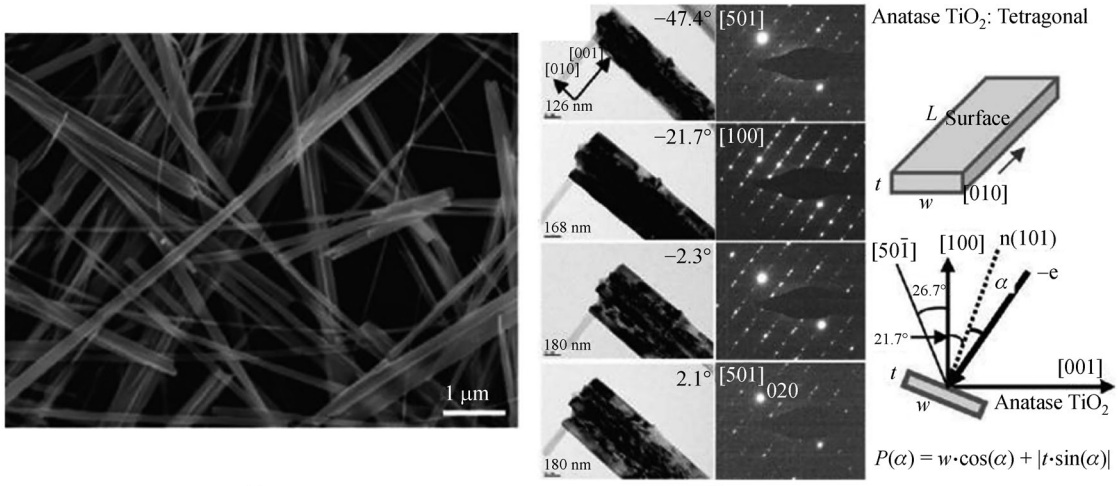

(a) (b)

Fig. 3 SEM and bright-field TEM images of TiO_2 nanobelts (reprinted with permission from Ref. [36]. Copyright 2010, American Chemical Society) (a) SEM image of the anatase TiO_2 nanobelts; (b) bright-field TEM images with SAED patterns of the nanobelt, and the diagram to show the relationship between the incident beam and the nanobelt

activity. For example, hierarchical yolk@shell microspheres with a hollow chamber that self-assembled by TiO_2 nanosheets (2–5 nm thickness) were synthesized, through a solvothermal process of organic amine-mediated alcoholysis of titanium (IV) precursor [37]. During the synthesis, carbon- and nitrogen-containing functional groups were simultaneously grafted onto the surface. With the special morphology, more energetic defective sites were generated on the interfaces to boost the reactivity. Meanwhile, the presence of carbon and nitrogen heteroatoms promoted the interaction and adsorption of CO_2 and narrowed the bandgap to enable visible light absorption. In the synthesis, the solvothermal temperature had an essential influence on the crystallinity and morphology of the catalyst, and no such catalysts could be attained below 160°C, which means the temperature must exceed this threshold to make the successful formation of the desired catalysts. Besides, additional calcination step in air was attempted after the solvothermal process, nevertheless, this extra step reduced the nitrogen content and the surface functional groups of the catalyst which showed inferior photocatalytic activity. The best-performed catalyst was obtained at a solvothermal temperature of 200°C without calcination, and methanol was the major product with a highest yield of 2.1 μmol/(g·h). The recycling tests were undertaken for this catalyst, which suggested that organic species might adsorb onto the catalyst surface and resulted in unsatisfactory catalytic stability, whereas it could be recovered by simply washing the catalyst after each run.

2.2 Black TiO_2

In 2011, a breakthrough was made by Mao's group in TiO_2-based photocatalysis [38]. In their work, a distinct strategy was adopted to synthesize visible light responsive TiO_2 materials, which introduced disorder in the surface layers of nanophase TiO_2 through hydrogenation. After hydrogenation, the outer layer (about 1 nm thickness) became disordered and the material color turned from white to black with substantially enhanced light harvesting into visible light and infrared range. The bandgap of black TiO_2 NPs prepared by a one-step reduction/crystallization displayed an estimated value of 1.85 eV. The unique crystalline and defective core/disordered shell morphology were the key factors in determining its electronic structure [39].

Black TiO_2 has been widely used in photocatalysis for organic pollutant decomposition, water splitting, etc [40–42]. In 2016, platinum (Pt) supported on black TiO_2 catalyst was developed using an impregnation method followed by hydrogenation, and was adopted for visible light photocatalytic reduction of CO_2 by CH_4 (CO_2 reforming of CH_4, abbreviated as CRM reaction) at elevated temperatures [43]. The Pt/black TiO_2 was further loaded onto the light-diffuse reflection surface of a silica dioxide (SiO_2) substrate, in order to significantly intensify light absorption capacity. High reaction temperature was introduced in the system because based on the relationship between band gap values and the redox potentials (see Fig. 4), high temperature altered the CO_2 redox potential to more easily produce CO. Simultaneously, the high temperature also favored the thermocatalytic reaction of CRM. Under the effects of supports and high temperature, exceptional H_2 and CO yields of 120.0 mmol/(g·h) and 270.0 mmol/(g·h) were achieved respectively under visible light irradiation at 650°C, with a high apparent quantum yield of 57.8%.

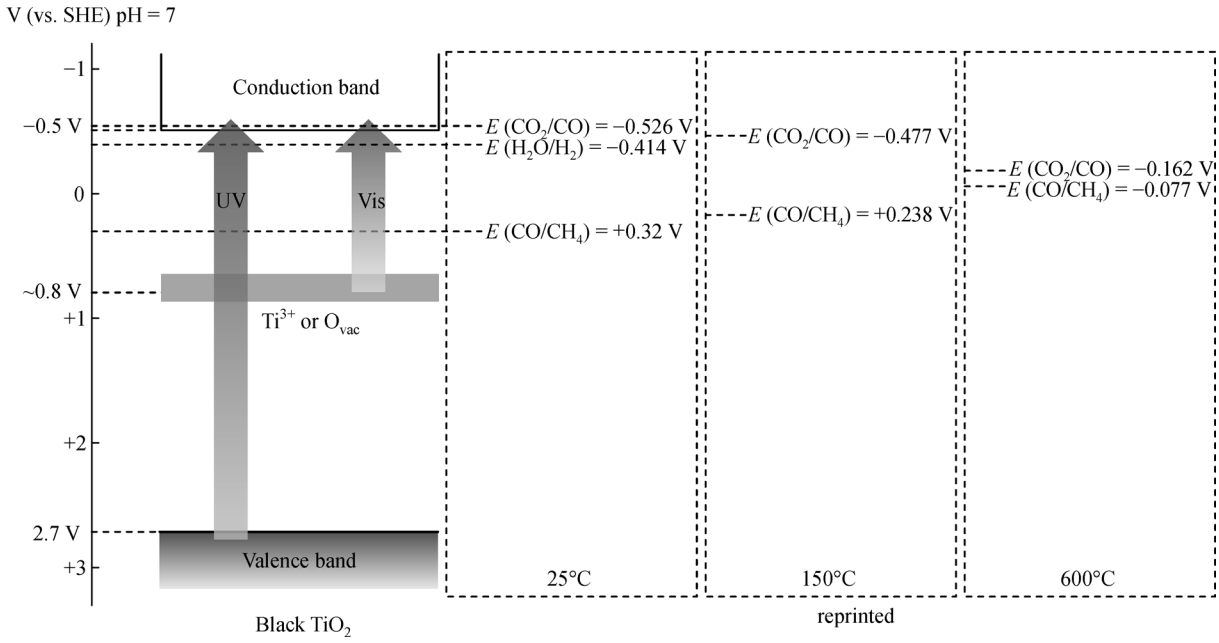

Fig. 4 Relationship between the bandgap and redox potentials of CRM (reprinted with permission from Ref. [43]. Copyright 2016, American Chemical Society)

3 TiO_2 modifications by incorporating other elements

The incorporation can use a single metal element or multiple metal elements as the co-catalysts. Table 1 summarizes the type of co-catalyst employed and their performances in CO_2 photoreduction.

3.1 Incorporation of a single metal element

The introduction of another element often imposes effects on the electron transfer and/or electron-hole separation, which modifies the reaction process. Noble metals were frequently used as the incorporating element to improve the performance of the commercialized TiO_2 (P25). In the following paragraphs, the TiO_2 referred to the P25 material if not specifically described. Yu et al. fabricated silver (Ag) NPs loaded TiO_2 by a simple silver mirror method with enhanced photocatalytic activity due to the surface plasmonic resonance (SPR) and electron sink effect of the Ag component [44]. The SPR promoted visible light absorption and generated hot electrons on Ag, while the photoexcited electrons transferred from the surface of TiO_2 to Ag concurrently because of the lower Fermi level. Hence, the electrons enriched on Ag surface to enhance the reduction capacity and retard the recombination of photogenerated electron-hole pairs. Since particle size influences the SPR, Ag NPs with a smaller size of 2–3 nm performed better than the larger NPs, reaching a CH_4 yield of 1.4 μmol/(g·h) under UV-vis light irradiation in the gas phase. When the photoreduction was conducted in aqueous phase, the major product was methanol with a yield of about 4.3 μmol/(g·h). Possible explanations (see Fig. 5) were given for the altered reaction pathway that CO_2 might undergo a chain of fast deoxygenation reactions in gas phase, whereas a chain of fast hydrogenation reactions occurred in aqueous phase because water existed in dominantly excessive amount.

Aside from noble metals, non-noble metals were also reported in TiO_2 modifications. Tahir and Amin fabricated indium (In)-incorporated TiO_2 NPs by a controlled sol-gel method [45]. The In mainly located on the surface of the NPs in its metallic state, which facilitated the formation of mesoporous anatase phase TiO_2 NPs with smaller crystalline sizes, increased surface areas, and enlarged bandgaps. The incorporation of In also enhanced charge separation and transfer, leading to a higher yield of CH_4 product in CO_2 photoreduction with water vapor. Corma's group reported copper (Cu)-modified TiO_2 NPs prepared by a solvothermal method [46]. The Cu^{2+} was incorporated into the crystal matrix of TiO_2, leading to a narrowed bandgap and an improved photocatalytic activity. Under UV-rich light, with Na_2S as the sacrificial electron donor, the Cu-doped catalyst promoted the reduction of CO_2 into formic acid with 25.7 μmol/(g·h) yield in aqueous solution at room temperature after 15 h reaction time. In another work, Cu-modified TiO_2 hollow microspheres were synthesized by a one-pot template-free method (see Fig. 6) [47]. The Cu element existed as copper oxide (CuO) and dominantly dispersed on the surface of the shell which did not insert into the crystal matrix of the anatase TiO_2. The large surface area and hierarchical porous structure of the hollow

Table 1 Summary of reviewed papers using co-catalysts to modify TiO_2

	Co-catalyst	TiO_2 type	Light source	S/%	Product	Production /(μmol·(g·h)$^{-1}$)	Ref.
1	Ag NPs	P25	UV-vis	-	CH_4 (gas) CH_3OH (aqueous)	1.4 4.3	[44]
2	In	P25	UV	69	CH_4	244.0	[45]
3	Cu	P25	UV-rich	-	HCOOH	25.7	[46]
4	CuO	P25	UV	-	CO	14.5	[47]
5	Cu^0	P25	UV	-	CH_4	30.1	[47]
6	Pt-Cu_2O	P25	UV-vis	85	CH_4	33.0	[48]
7	Pt-MgO	P25	UV-vis	83	CH_4	8.9	[49]
8	Au-Cu	P25	Smulated sunlight	97	CH_4	2000	[50]
9	Cu-Pt	P25	UV-vis	-	CH_4	11.4	[51]
10	Pt-Cu_2O	TiO_2 NCs	UV	97	CH_4	1.4	[52]
11	Au-Cu	$SrTiO_3/TiO_2$	UV-vis	-	CH_4	421.2	[53]
12	Cu-Pt	TiO_2 NTAs	Simulated sunlight	-	CH_4	0.6	[54]
13	Au	TiO_2 NTAs	Simulated sunlight	-	CH_4	58.5	[55]
14	Ru	TiO_2 NTAs	Simulated sunlight	-	CH_4	26.4	[55]
15	Zn-Pd	TiO_2 NTAs	Simulated sunlight	-	CH_4	26.8	[55]
16	Ag-Pd	N-doped TiO_2 NSs	Simulated sunlight	-	CH_4	79.0	[56]
17	Cu-In	P25	UV	99	CO	6.5	[58]
18	Ni-In	P25	UV	99.7	CO	12.0	[59]
19	Au-In	P25	UV	99	CO	9.0	[57]
20	Cu-In	TiO_2 NPs	UV	92 66	CH_4 CH_3OH	181.0 68.0	[60]
21	Cu-V	P25 & PU	Visible	-	CH_4 CO	933.0 588.0	[61]

Notes: NTA—nanotube arrays; NCs—nanocrystals; NSs—nanosheets; S%—selectivity%

microspheres enhanced the light harvesting of the catalyst, and the introduction of CuO improved the electron trapping ability. The 3 wt% CuO doped TiO_2 hollow microsphere catalyst afforded a higher CO yield of 14.5 μmol/(g·h), which was 5.8 times than that of using undoped counterpart catalyst under UV light irradiation. Besides, Cu^0 doped TiO_2 hollow microsphere catalyst was obtained by hydrogenating the CuO-doped TiO_2 catalyst, which promoted selective reduction of CO_2 into CH_4 with a yield of 30.1 μmol/(g·h), because Cu^0 favored the capture of holes and the H_2 generation from water for CH_4 formation.

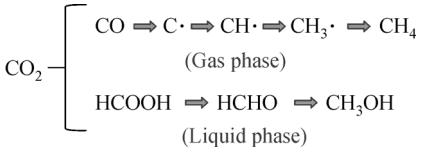

Fig. 5 Proposed reaction pathways for the selective photoreduction of CO_2 into different products in gas and liquid phase respectively (adapted with permission from Ref. [44]. Copyright 2016, Royal Society of Chemistry)

3.2 Incorporation of dual metal co-catalysts

Wang's group reported the binary co-catalysts $Cu_2O/Pt/TiO_2$ system and MgO (magnesium oxide)-Pt/TiO_2 system for selective photoreduction of CO_2 into CO and CH_4 with water (at 50°C, 2 bar CO_2 pressure) under UV-vis light irradiation [48,49]. The catalysts were synthesized by a stepwise photodeposition technique with Pt NPs/TiO_2 formed first. Then, Cu_2O was preferentially deposited on the Pt NPs forming a core-shell structure, while MgO was deposited onto the TiO_2 as amorphous layers. The major role of Pt NPs as a co-catalyst was to capture and enrich the photogenerated electrons as well as to delay the electron-hole recombination. Nevertheless, Pt NPs promoted H_2 formation significantly and led to low selectivity toward CO_2 reduction. Incorporating Cu_2O or MgO remarkably curbed the competing reaction of H_2 generation and facilitated the chemisorption and activation of CO_2. Hence, $Cu_2O/Pt/TiO_2$ and MgO-Pt/TiO_2 catalysts achieved a high selectivity of 85% and 83% respectively, which were 2-fold of that using pristine TiO_2 or Pt/TiO_2. The highest yield of CH_4 was obtained at about 33.0 μmol/(g·h) with

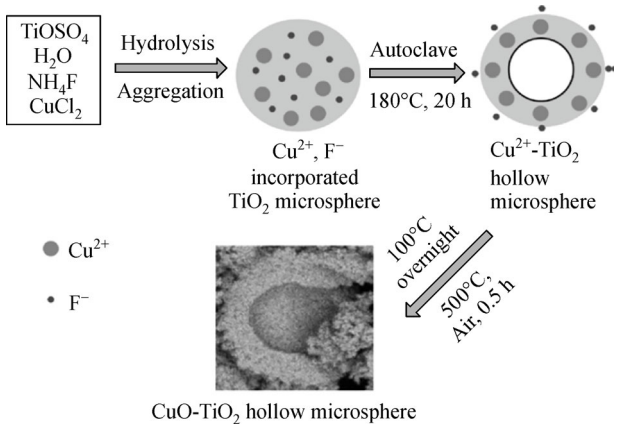

Fig. 6 Synthesis method to prepare CuO-TiO_2 hollow microsphere (reprinted with permission from Ref. [47]. Copyright 2015, American Chemical Society)

$Cu_2O/Pt/TiO_2$. Moreover, the reaction mode was proved to considerably affect the product yield, and higher CH_4 yield was achieved in gas phase reaction mode presumably because of the low solubility of CO_2 in water and the more severe side reaction in liquid water (see Fig. 7). Meanwhile, the synthesis method played a role in the catalytic performance that the catalysts obtained by the photodeposition method exhibited a better activity than those prepared by the impregnation H_2-reduction method and the hydrazine-reduction method.

Garcia's group developed the gold-copper (Au-Cu)/TiO_2 catalyst for photoreduction of CO_2 by water under simulated concentrate sunlight [50]. The Au-Cu bimetallic alloy NPs were fabricated by a stepwise deposition-precipitation method. The catalyst realized 97% of selectivity toward CH_4, and a high production rate of about 2000 μmol/(g·h) that was about 10 times of those using Au/TiO_2 or Cu/TiO_2 counterparts. Surface species were probed by using FTIR and chemical analysis, including $CO_2^{\bullet-}$, Cu-CO, and elemental carbon. As proposed, the role of Au was to induce the visible light responses, and the Cu adsorbed CO as an intermediate and governed the reduction pathway. The type of excitation lights played a crucial role in reaction pathways that UV light irradiation promoted the H_2 evolution reaction whereas visible light illumination led to the generation of CH_4 product (see Fig. 8). Afterwards, Cu-Pt bimetallic alloy NPs supported on TiO_2 was developed by an impregnation-calcination method, and the size effect of the Cu-Pt nanoalloys were studied [51]. As the particle size decreased, the production yield of CH_4 correspondingly increased. The highest yield of 11.4 μmol/(g·h) was obtained when the size of Cu-Pt NPs was 1.2 nm under UV-vis light irradiation at 40°C. Several reasons were proposed for the size-dependent photoreduction of CO_2. First, catalysts with smaller size might possess stronger reductive powder due to more quantized energy level, and enhanced binding capacity of CO_2 with increased low-coordinated sites. Moreover, Cu-Pt NPs with a smaller size probably had reinforced interaction with the TiO_2 support, which possibly enabled the co-adsorption of intermediates with –OH groups on the support. Besides, the Pt atoms of smaller Cu-Pt NPs were observed to show a stronger adsorption of protons for hydrogenation of intermediates.

Cu_2O NPs and Pt NPs decorated on TiO_2 nanocrystals with coexposed (101) and (001) facets were synthesized [52]. The facet-engineered TiO_2 support was obtained by a solvothermal method and the NPs were prepared by a sodium borohydride ($NaBH_4$) reduction method. The

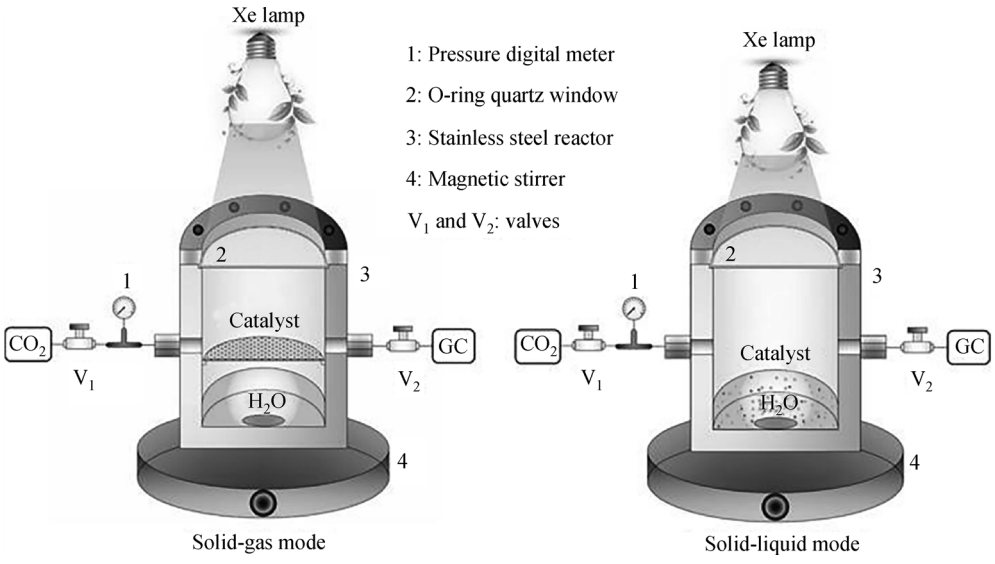

Fig. 7 Schematic diagrams of different reaction modes for photocatalytic reduction of CO_2 (reprinted with permission from Ref. [49]. Copyright 2014, American Chemical Society)

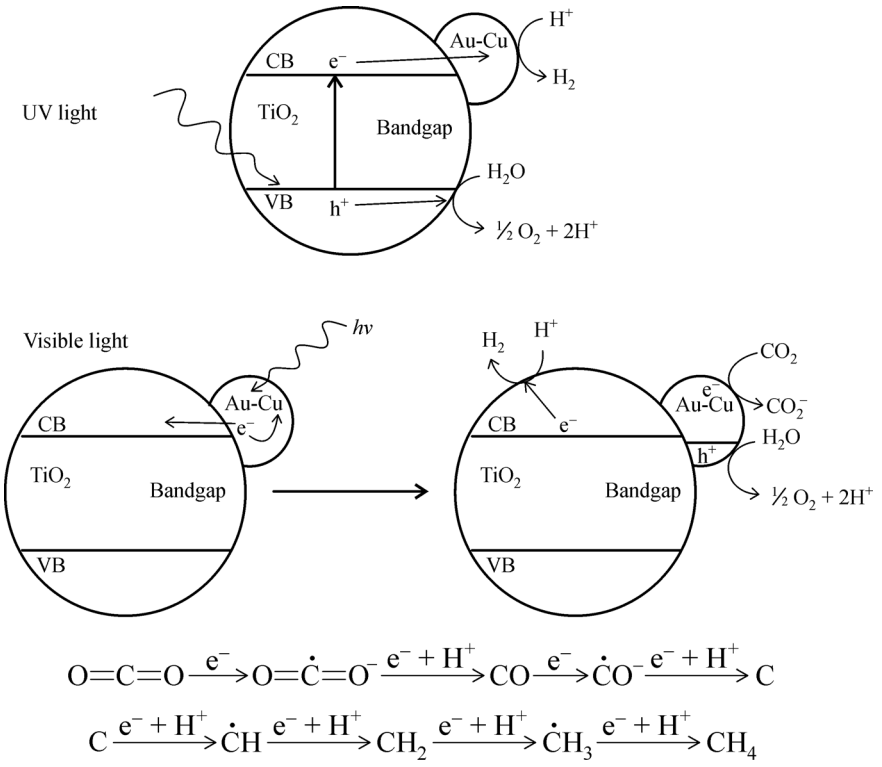

$$O{=}C{=}O \xrightarrow{e^-} O{=}\dot{C}{=}O^- \xrightarrow{e^- + H^+} CO \xrightarrow{e^-} \dot{C}O^- \xrightarrow{e^- + H^+} C$$

$$C \xrightarrow{e^- + H^+} \dot{C}H \xrightarrow{e^- + H^+} CH_2 \xrightarrow{e^- + H^+} \dot{C}H_3 \xrightarrow{e^- + H^+} CH_4$$

Fig. 8 Proposal mechanism to explain the different product distribution under different types of light sources using $AuCu/TiO_2$ catalyst for photoreduction of CO_2 by water (reprinted with permission from Ref. [50]. Copyright 2014, American Chemical Society)

catalyst system significantly suppressed H_2 production, improving the selectivity toward CH_4 to 97% under UV light irradiation. The Cu_2O NPs showed a poor adsorption toward water and thus inhibited the competing reaction, whereas they displayed enhanced chemisorption of CO_2 by Cu_2O NPs as verified by temperature programmed desorption (TPD)-CO_2. Meanwhile, Pt NPs were found to not only extract the photogenerated electrons but also increase the electron density on Cu_2O for selective eight-electron reduction of CO_2 into CH_4. Control experiments suggested that CH_4 was primarily produced via the direct photocatalytic reduction of CO_2, instead of the hydrogenation of CO/CO_2. Likewise, special supports such as amorphous $SrTiO_3/TiO_2$ coaxial nanotube arrays were employed by Kang et al. with Au-Cu bimetallic alloys as the co-catalysts [53]. The support material could enhance the gas diffusion with its porosity and high surface area and promoted the photogenerated charge separation thanks to its heterostructures. Besides, hydrous hydrazine was used as the reducing agent which exhibited better reductive capacity and offered a protective atmosphere for the Au-Cu NPs. Under UV-vis light irradiation, the highest CH_4 yield was obtained at 421.2 μmol/(g·h) from diluted CO_2 stream with Au_3Cu co-catalysts. It was believed that the Au atom facilitated the desorption of CO and boosted the formation of hydrocarbons on the Cu atom, and the proposed mechanism mainly followed the glyoxal pathway.

Cu-Pt NPs supported on TiO_2 nanotube arrays were prepared, with an emphasis on the influence of synthesis methods [54]. The transparent 1D TiO_2 nanotube arrays as support provided more reaction sites and co-catalyst loading sites due to the high surface area. The photodeposited Cu-Pt NPs have an average size of about 1 nm, and a Schottky barrier was formed at the co-catalyst-TiO_2 interface with an obvious band bending. Nevertheless, sputtered and thermally dewetted Cu-Pt NPs had larger particle sizes and the band bending was not observed. Using the photodeposition method, a higher CH_4 yield of about 0.6 μmol/(cm^2·h) could be achieved which was nearly 20-fold than that when sputtered Cu-Pt NPs catalysts were used. In a following work, the group also synthesized Au, ruthenium (Ru), and zinc-palladium (Zn-Pd) NPs loaded TiO_2 nanotube arrays and examined their photocatalytic activity for CO_2 reduction [55]. Au NPs on the support generated CH_4 at the highest yield of 58.5 μmol/(g·h) possibly because of its smallest particle size. The metal NPs loaded TiO_2 nanotube arrays could not only utilize UV protons but also the blue photons. Tan et al. prepared Ag-Pd bimetallic alloys on nitrogen-doped (N-doped) TiO_2 nanosheets by a hydrazine-reduction method [56]. The doping of nitrogen into the nanosheets could favor charge separation and boost visible light absorption. By means of combined analytical methods, the well-dispersed Ag-Pd NPs (having a diameter of about 8.5 nm)

facilitated visible-light response, charge transfer and separation, as well as the activation of CO_2. The ratio of Ag and Pd was optimized and a linear growth of the product was found with the prolonged reaction time (see Figs. 9(a) and 9(b)). When simulating sunlight irradiation, the highest CH_4 yield of 79.0 μmol/(g·h) was obtained by using Ag-Pd/TiO_2 nanosheets in CO_2-saturated aqueous solution at room temperature and ambient pressure, which was 3-fold higher than using monometallic counterparts, and recycling tests were conducted to show the stability of the catalysts (see Figs. 9(c) and 9(d)).

Amin's group developed a series of dual components-incorporated TiO_2 catalysts (Cu-In, nickel (Ni)-In, Au-In) using the sol-gel method for the photocatalytic reduction of CO_2 into CO with H_2 reductant in a monolith reactor [57–59]. The dual elements displayed synergistic effects and significantly inhibited the recombination of photogenerated electron-hole pairs. In these catalysts, the elements located at the surface and existed as Cu^+ and In^{3+} (Cu-In co-doped), Ni^{2+} and In^{3+} (Ni-In co-doped), and Au^0 and In^{3+} (Au-In co-doped). The selectivity toward the CO product for these three co-doped catalysts were 99.3%, 99.7%, and 99.0% respectively, with the highest yields of 6.5, 12.0 and 9.0 mmol/(g·h). In a following work, In and Cu-decorated TiO_2 NPs with surface dispersed In^{3+} and Cu^{2+} were obtained by using the modified sol-gel method [60]. After the introduction of the two elements, the catalyst boasted smaller crystalline size, reduced bandgap, and enhanced charge separation, which resulted in a better CO_2 photoreduction activity. Under optimal conditions, CH_4 was formed at the highest yield of 181.0 μmol/(g·h) with water as the reductant, and methanol was formed at the highest yield of 68.0 μmol/(g·h) with water and H_2 as the reductants. On the other hand, the introduction of a metal element and a non-metal element was exploited. Cu-vanadium (V) modified TiO_2 was synthesized and supported on porous polyurethane (PU) with a honeycomb structure [61]. The use of support was to ease the recycling and increase the adsorption ability. The Cu element presented as Cu^+ and Cu^{2+} species either on the surface or in the matrix. The V element existed as V^{4+} and V^{5+} species, with V^{4+} species incorporating into the lattice while V^{5+} species distributing on the surface. The Cu and V elements have induced the generation of Ti^{3+} and oxygen vacancies in the lattice, leading to an enhanced charge separation and CO_2 adsorption. Under visible light

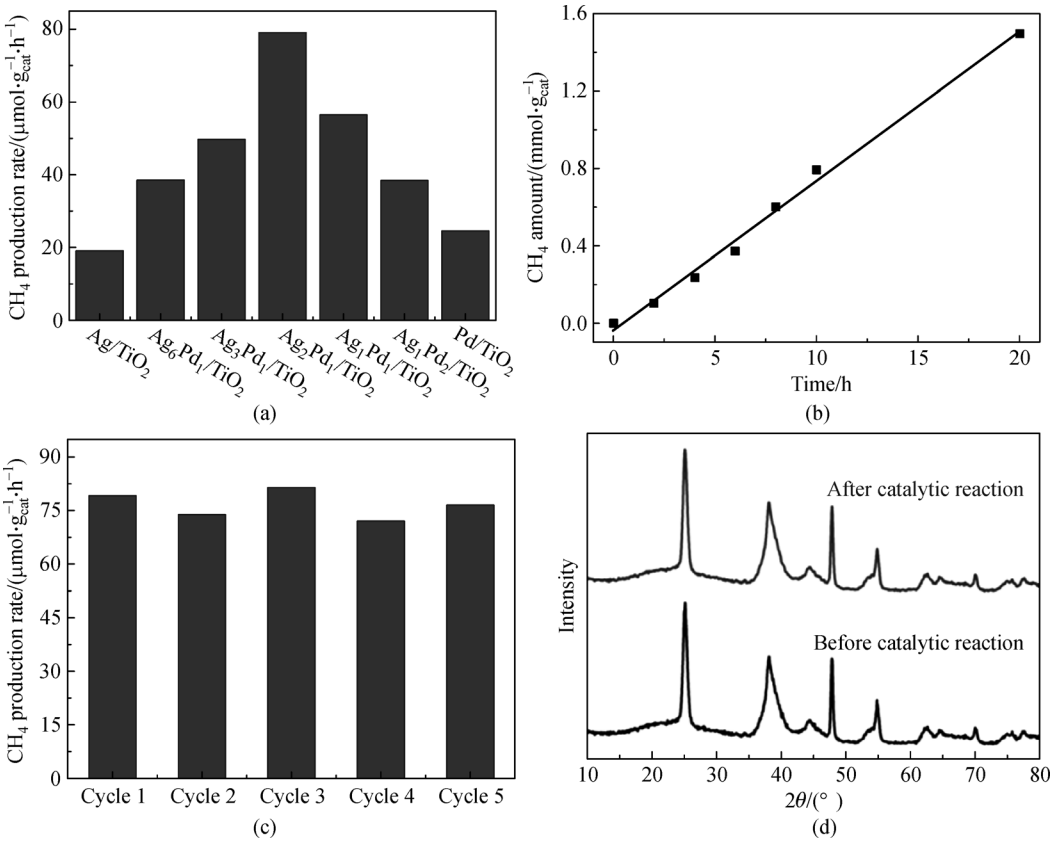

Fig. 9 Optimization, recycling tests and XRD analysis of Ag-Pd/TiO_2 nanosheets
(a) Optimization of Ag/Pd ratios; (b) time-dependent production of CH_4; (c) recycling tests for 5 cycles; (d) XRD patterns of the photocatalyst after use (reprinted with permission from Ref. [56]. Copyright 2018, American Chemical Society)

irradiation, CO_2 was efficiently reduced with water vapor into CH_4 and CO with the production rates of 933.0 μmol/(g·h) and 588.0 μmol/(g·h).

4 TiO_2 modifications by non-metal elements

Apart from metal elements, non-metal elements were also used to modify the structure of TiO_2 to increase its visible light responses and CO_2 adsorption ability. For example, N-doped TiO_2 materials were widely used as photocatalysts [62]. Liu's group synthesized N-doped anatase TiO_2 microsheets with exposed (001) and (101) facets by using the hydrothermal method with HF and hydrochloric acid (HCl) using titanium nitride (TiN) as the precursor. The N-doped microsheets exhibited a much enhanced activity than undoped TiO_2 for CO_2 photoreduction into CH_4 [63]. Zhang et al. fabricated 1D N-doped TiO_2 nanorod arrays by a hydrothermal treatment using hydrazine or ammonia as the nitrogen source, and pointed out that the use of different nitrogen source had an impact on the selectivity of CO_2 photoreduction [64]. The major product was CH_4 and CO respectively when using hydrazine and ammonia as the source, probably because of the highly reductive N-N bonds introduced by hydrazine. In addition, hierarchical phosphate-doped (P-doped) TiO_2 nanotubes were prepared and supported on Ti plates by simple pyrolytic phosphating and electrochemical anodic oxidation [65]. Hierarchical nanostructures would enhance the mass transfer and light harvesting. The incorporated P^{5+} fractionally substituted Ti^{4+} atoms in the crystal lattice to form Ti-O-P linkages, suppressing recombination rate of photogenerated electron-hole pairs. Besides, the P-doped material boasted a reduced bandgap, a higher activity, and a better selectivity. Under visible light irradiation, the maximal methanol yield was obtained at 286.8 μmol/(g·h) by using water vapor as the reducing agent.

Sulfur-doped (S-doped) TiO_2 anatase was synthesized by using the sonothermal method, and S atoms were predominantly incorporated as S^{4+} in the crystal lattice [66]. By DFT calculations, S-doping induced the generation of additional states in the bandgap closer to the VB, and presumably enhanced the surface conductivity, the charge transfer efficiency, and the photocatalytic activity. Under visible light irradiation, a production of 35.3 μmol/(g·h) of CH_4 and 167.9 μmol/(g·h) of methanol was achieved in basic acetonitrile-water solution (CO_2-saturated) with triethanolamine (TEOA) as sacrificial donor. Moreover, iodine-doped (I-doped) TiO_2 nanosheets with high exposed (001) facets were developed by a two-step hydrothermal treatment followed by calcinations [67]. After doping, Ti^{4+} replacement by I^{5+} was observed with the formation of I-O-Ti and I-O-I bonds, leading to increased visible light responses. Meanwhile, the high exposed (001) facets favored water oxidation and the increased unsaturated Ti atoms curbed the recombination rate of electron-hole pairs. In gas phase, CH_4 and CO were obtained at the yields of 9.1 μmol/(g·h) and 3.4 μmol/(g·h) respectively under visible light irradiation.

5 Multi-component hybrid TiO_2 nanocomposites

Structurally blended TiO_2 with carbon-based materials along with the addition of co-catalysts and/or other elements was employed in some studies to fabricate a hybrid nanocomposite in an effort to further utilize the synergistic effects among multiple components and improve the photocatalytic activity and/or stability. TiO_2-graphene hybrid nanosheets were established by an *in situ* reduction-hydrolysis technique in ethylenediamine/water solvent [68]. The TiO_2 NPs were chemically loaded onto graphene sheets via Ti-O-C linkages and generated a two-dimension (2D) sandwich-like nanostructure. The loaded TiO_2 NPs stabilized the graphene nanosheets preventing them from restacking or collapsing. Abundant Ti^{3+} sites were identified at the surface of TiO_2 NP in hybrid composites which could trap electrons and suppressed photogenerated electron-hole recombination. The hybrid composites selectively promoted the formation of C_2H_6 product, which was distinct from the single component counterparts. Besides, the yield of C_2H_6 correspondingly grew with the increased ratio of graphene in the composite, indicating that the construction of a hybrid composite might provide a facile way to adjust the reaction selectivity.

A hybrid RuRe/TiO_2/graphic carbon nitride (g-C_3N_4) nanosheet was contrived by first anchoring a supramolecular Ru(II)-Re(I) binuclear complex onto rutile TiO_2 NPs which were then coated on g-C_3N_4 nanosheets [69]. The band structure of the hybrid catalyst is shown in Fig. 10. The hybrid composites showed superior photocatalytic activity to the analog without TiO_2 in CO_2 reduction to produce CO, which demonstrated about 4-fold production rate and turnover number (TON). The improved photocatalytic activity was ascribed to the enhanced charge separation efficiency at the interface of TiO_2 and g-C_3N_4, as indicated by the results from transient absorption spectroscopy. Moreover, the TiO_2 NPs offered stronger sites to anchor the RuRe complexes than the carbon materials, leading to a better hybrid structure. These two factors in combination determined the improved performances of the hybrid composites.

Jin et al. utilized a Cu-TiO_2/g-C_3N_4 ternary photocatalyst for CO_2 reduction to CH_4 with water vapor under visible light irradiation [70]. The interface heterojunctions of the ternary system could efficiently boost the charge separation. Cu-loaded TiO_2 NPs were first prepared by a

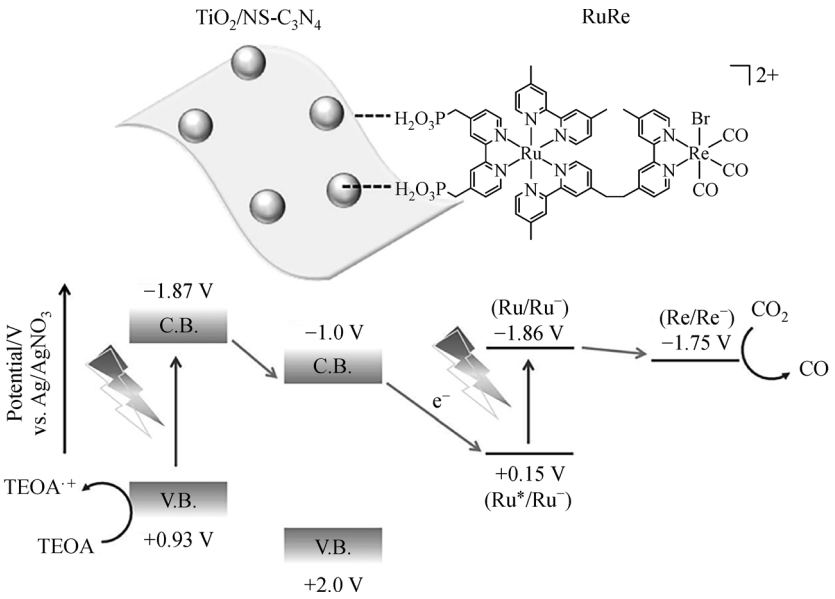

Fig. 10 Band structure of RuRe/TiO_2/g-C_3N_4 hybrid nanosheets (reprinted with permission from Ref. [69]. Copyright 2017, American Chemical Society)

$NaBH_4$ reduction process, and then the composites were dispersed on g-C_3N_4 by stirring and annealing. The small Cu NPs were in metallic state and well-dispersed on the surface of TiO_2 NPs, which promoted light absorption. Cu loading was identified as a critical factor to influence the photocatalytic activity with an optimal value of 2.5 wt%, which achieved CH_4 formation at a rate of 23.9 μmol/(g·h). The reaction mechanism was proposed that the photoexcited electrons were initially injected from the VB to CB of g-C_3N_4, and then migrated to the CB of TiO_2 which eventually accumulated at Cu sites for efficient CO_2 reduction.

Similarly, a Ag-TiO_2/g-C_3N_4 catalyst was developed by adopting simple solvent evaporation-calcination processes [71]. The remarkable synergy among the components led to increased light harvesting and charge separation to more effectively reduce CO_2 into CH_4 and CO at simulated sunlight illumination. Photogenerated electrons were presumably transferred in this way g-C_3N_4 → TiO_2 → Ag, and the collected electrons were further reinforced by the SPR effect. The multicomponent catalyst of Pt/CoO_x/TiO_2-SiO_2 were synthesized [72] to demonstrate the spatial influence of the catalyst. Pt NPs and CoO_x NPs were anchored at separated spatial locations on hierarchically ordered TiO_2-SiO_2 (HTSO) support which advanced the separation of charge carriers. The HTSO was prepared by the two template evaporate induced self-assemble (EISA) method, and CoO_x NPs were *in situ* grown and embedded in the skeleton of the support during its formation. Afterwards, Pt NPs were decorated onto the outer surface of HTSO. The Pt NPs acted as electron reservoirs while CoO_x NPs were effective hole collectors, and the physical isolation of the two co-catalysts notably retarded the recombination rate of photoexcited electron-hole pairs because the possibility of an electron recombined with a hole were reduced by the prolonged distance. Compared to randomly dispersed Pt-CoO_x with contacts, spatially separated Pt NPs and CoO_x NPs on HTSO exhibited a higher activity and selectivity to produce CH_4 from CO_2 at simulated solar light illumination. In addition, the composition, porous structure and specific surface area of the support are influential to the photocatalytic performance by mediating the light reflection, mass transfer, electron-hole recombination rate, etc [53–56].

6 Conclusions and future remarks

Photocatalytic reduction of CO_2 has attracted growing attention recently because it exploits clean and renewable solar energy to create fuels, which decreases the dependence on depleting fossil oils and points out a potentially low-carbon future for the sustainable development. TiO_2-based materials are economically viable as photocatalysts because of its cheap price and high stability. The key factors affecting the performances of CO_2 photoreduction mainly include the surface affinity, charge separation efficiency, and the light absorption ability of the catalyst employed. Surface affinity determines the adsorption of CO_2 on the surface of the catalyst, while a strong affinity can help improve the selectivity toward CO_2 conversion and suppress the side reaction, which will influence both the selectivity and yield. A common strategy to improve the affinity is to incorporate basic

sites onto the surface. The charge separation efficiency and the light absorption ability are crucially associated with the quantum yields and product yields.

Although various methods have been used to enhance the performance of TiO_2 catalysts, the production rate of photocatalytic reduction of CO_2 is relatively low compared to conventional chemical transformations. Major challenges in CO_2 photoreduction include the further enhancement in product yields, the efficiency of electron-hole separation, and the light harvesting efficiency. Therefore, in the future, different effective and cooperative strategies are anticipated to be developed to considerably increase the CO_2 reduction efficiency and the production rate. For instance, the combined uses of photocatalysis and thermal catalysis may lead to much enhanced results [73]. In addition, the manipulations on reactors and reaction modes can be further studied and optimized in detail to adjust the process conditions. Besides, more rational and elaborate catalyst design is always essential to achieve highly selective reduction of CO_2 with solar lights.

Acknowledgements This work was financially supported by the State Key Program of the National Natural Science Foundation of China (Grant Nos. 21436007 and 51472159).

References

1. Frölicher T L, Fischer E M, Gruber N. Marine heatwaves under global warming. Nature, 2018, 560(7718): 360–364
2. Dottori F, Szewczyk W, Ciscar J C, Zhao F, Alfieri L, Hirabayashi Y, Bianchi A, Mongelli I, Frieler K, Betts R A, Feyen L. Increased human and economic losses from river flooding with anthropogenic warming. Nature Climate Change, 2018, 8(9): 781–786
3. Peters G P, Andrew R M, Boden T, Canadell J G, Ciais P, Le Quéré C, Marland G, Raupach M R, Wilson C. The challenge to keep global warming below 2°C. Nature Climate Change, 2013, 3(1): 4–6
4. Earth System Research Laboratory. Trends in Atmospheric Carbon Dioxide. Global Greenhouse Gas Reference Network, 2019
5. Buelens L C, Galvita V V, Poelman H, Detavernier C, Marin G B. Super-dry reforming of methane intensifies CO_2 utilization via Le Chatelier's principle. Science, 2016, 354(6311): 449–452
6. Senftle T P, Carter E A. The Holy Grail: Chemistry enabling an economically viable CO_2 capture, utilization, and storage strategy. Accounts of Chemical Research, 2017, 50(3): 472–475
7. Meylan F D, Moreau V, Erkman S. CO_2 utilization in the perspective of industrial ecology, an overview. Journal of CO_2 Utilization, 2015, 12: 101–108
8. Zhai H, Ou Y, Rubin E S. Opportunities for decarbonizing existing U.S. coal-fired power plants via CO_2 capture, utilization and storage. Environmental Science & Technology, 2015, 49(13): 7571–7579
9. Olajire A A. Valorization of greenhouse carbon dioxide emissions into value-added products by catalytic processes. Journal of CO_2 Utilization, 2013, 3–4: 74–92
10. Moret S, Dyson P J, Laurenczy G. Direct synthesis of formic acid from carbon dioxide by hydrogenation in acidic media. Nature Communications, 2014, 5(1): 4017
11. Goeppert A, Czaun M, Jones J P, Surya Prakash G K, Olah G A. Recycling of carbon dioxide to methanol and derived products – closing the loop. Chemical Society Reviews, 2014, 43(23): 7995–8048
12. Qiao J, Liu Y, Hong F, Zhang J. A review of catalysts for the electroreduction of carbon dioxide to produce low-carbon fuels. Chemical Society Reviews, 2014, 43(2): 631–675
13. Lewis N S, Nocera D G. Powering the planet: chemical challenges in solar energy utilization. Proceedings of the National Academy of Sciences of the United States of America, 2006, 103(43): 15729–15735
14. Inoue T, Fujishima A, Konishi S, Honda K. Photoelectrocatalytic reduction of carbon dioxide in aqueous suspensions of semiconductor powders. Nature, 1979, 277(5698): 637–638
15. Low J, Cheng B, Yu J. Surface modification and enhanced photocatalytic CO_2 reduction performance of TiO_2: a review. Applied Surface Science, 2017, 392: 658–686
16. White J L, Baruch M F, Pander J E III, Hu Y, Fortmeyer I C, Park J E, Zhang T, Liao K, Gu J, Yan Y, Shaw T W, Abelev E, Bocarsly A B. Light-driven heterogeneous reduction of carbon dioxide: photocatalysts and photoelectrodes. Chemical Reviews, 2015, 115 (23): 12888–12935
17. Habisreutinger S N, Schmidt-Mende L, Stolarczyk J K. Photocatalytic reduction of CO_2 on TiO_2 and other semiconductors. Angewandte Chemie International Edition, 2013, 52(29): 7372–7408
18. Sakakura T, Choi J C, Yasuda H. Transformation of carbon dioxide. Chemical Reviews, 2007, 107(6): 2365–2387
19. Wang W, Wang S, Ma X, Gong J. Recent advances in catalytic hydrogenation of carbon dioxide. Chemical Society Reviews, 2011, 40(7): 3703–3727
20. Roy S C, Varghese O K, Paulose M, Grimes C A. Toward solar fuels: photocatalytic conversion of carbon dioxide to hydrocarbons. ACS Nano, 2010, 4(3): 1259–1278
21. Kim W, McClure B A, Edri E, Frei H. Coupling carbon dioxide reduction with water oxidation in nanoscale photocatalytic assemblies. Chemical Society Reviews, 2016, 45(11): 3221–3243
22. Zhang L, Zhao Z J, Gong J. Nanostructured materials for heterogeneous electrocatalytic CO_2 reduction and their related reaction mechanisms. Angewandte Chemie International Edition, 2017, 56(38): 11326–11353
23. Ma K, Tian Y, Zhao Z J, Cheng Q, Ding T, Zhang J, Zheng L, Jiang Z, Abe T, Tsubaki N, Gong J, Li X. Achieving efficient and robust catalytic reforming on dual-sites of Cu species. Chemical Science (Cambridge), 2019, 10(9): 2578–2584
24. Li Z, Qu Y, Wang J, et al. Highly selective conversion of carbon dioxide to aromatics over tandem catalysts. Joule, 2019, 3(2): 570–580
25. Wang Y, Zhang Z, Zhang L, Luo Z, Shen J, Lin H, Long J, Wu J C S, Fu X, Wang X, Li C. Visible-light driven overall conversion of CO_2 and H_2O to CH_4 and O_2 on 3D-SiC@2D-MoS_2 heterostructure. Journal of the American Chemical Society, 2018, 140(44): 14595–14598
26. Kawahara T, Konishi Y, Tada H, Tohge N, Nishii J, Ito S. A patterned TiO_2 (anatase)/TiO_2 (rRutile) bilayer-type photocatalyst: effect of the anatase/rutile junction on the photocatalytic activity.

Angewandte Chemie, 2002, 114(15): 2935–2937
27. Ohno T, Tokieda K, Higashida S, Matsumura M. Synergism between rutile and anatase TiO_2 particles in photocatalytic oxidation of naphthalene. Applied Catalysis A, General, 2003, 244(2): 383–391
28. Kandiel T A, Dillert R, Feldhoff A, Bahnemann D W. Direct synthesis of photocatalytically active rutile TiO_2 nanorods partly decorated with anatase nanoparticles. Journal of Physical Chemistry C, 2010, 114(11): 4909–4915
29. Tan L L, Ong W J, Chai S P, Mohamed A R. Visible-light-activated oxygen-rich TiO_2 as next generation photocatalyst: importance of annealing temperature on the photoactivity toward reduction of carbon dioxide. Chemical Engineering Journal, 2016, 283: 1254–1263
30. Reñones P, Moya A, Fresno F, Collado L, Vilatela J J, de la Peña O'Shea V A. Hierarchical TiO_2 nanofibres as photocatalyst for CO_2 reduction: influence of morphology and phase composition on catalytic activity. Journal of CO_2 Utilization, 2016, 15: 24–31
31. Han X, Kuang Q, Jin M, Xie Z, Zheng L. Synthesis of titania nanosheets with a high percentage of exposed (001) facets and related photocatalytic properties. Journal of the American Chemical Society, 2009, 131(9): 3152–3153
32. Yang H G, Sun C H, Qiao S Z, Zou J, Liu G, Smith S C, Cheng H M, Lu G Q. Anatase TiO_2 single crystals with a large percentage of reactive facets. Nature, 2008, 453(7195): 638–641
33. Selloni A. Anatase shows its reactive side. Nature Materials, 2008, 7 (8): 613–615
34. Yu J, Low J, Xiao W, Zhou P, Jaroniec M. Enhanced photocatalytic CO_2-reduction activity of anatase TiO_2 by coexposed {001} and {101} facets. Journal of the American Chemical Society, 2014, 136 (25): 8839–8842
35. Liu L, Jiang Y, Zhao H, Chen J, Cheng J, Yang K, Li Y. Engineering coexposed {001} and {101} facets in oxygen-deficient TiO_2 nanocrystals for enhanced CO_2 photoreduction under visible light. ACS Catalysis, 2016, 6(2): 1097–1108
36. Wu N, Wang J, Tafen D N, Wang H, Zheng J G, Lewis J P, Liu X, Leonard S S, Manivannan A. Shape-enhanced photocatalytic activity of single-crystalline anatase TiO_2 (101) nanobelts. Journal of the American Chemical Society, 2010, 132(19): 6679–6685
37. Liu S, Xia J, Yu J. Amine-functionalized titanate nanosheet-assembled Yolk@Shell microspheres for efficient cocatalyst-free visible-light photocatalytic CO_2 reduction. ACS Applied Materials & Interfaces, 2015, 7(15): 8166–8175
38. Chen X, Liu L, Yu P Y, Mao S S. Increasing solar absorption for photocatalysis with black hydrogenated titanium dioxide nanocrystals. Science, 2011, 331(6018): 746–750
39. Naldoni A, Allieta M, Santangelo S, Marelli M, Fabbri F, Cappelli S, Bianchi C L, Psaro R, Dal Santo V. Effect of nature and location of defects on bandgap narrowing in black TiO_2 nanoparticles. Journal of the American Chemical Society, 2012, 134(18): 7600–7603
40. Hu Y H. A highly efficient photocatalyst—hydrogenated black TiO_2 for the photocatalytic splitting of water. Angewandte Chemie International Edition, 2012, 51(50): 12410–12412
41. Cui H, Zhao W, Yang C, Yin H, Lin T, Shan Y, Xie Y, Gu H, Huang F. Black TiO_2 nanotube arrays for high-efficiency photoelectrochemical water-splitting. Journal of Materials Chemistry. A, Materials for Energy and Sustainability, 2014, 2(23): 8612–8616
42. Leshuk T, Parviz R, Everett P, Krishnakumar H, Varin R A, Gu F. Photocatalytic activity of hydrogenated TiO_2. ACS Applied Materials & Interfaces, 2013, 5(6): 1892–1895
43. Han B, Wei W, Chang L, Cheng P, Hu Y H. Efficient visible light photocatalytic CO_2 reforming of CH_4. ACS Catalysis, 2016, 6(2): 494–497
44. Yu B, Zhou Y, Li P, Tu W, Li P, Tang L, Ye J, Zou Z. Photocatalytic reduction of CO_2 over Ag/TiO_2 nanocomposites prepared with a simple and rapid silver mirror method. Nanoscale, 2016, 8(23): 11870–11874
45. Tahir M, Amin N S. Indium-doped TiO_2 nanoparticles for photocatalytic CO_2 reduction with H_2O vapors to CH_4. Applied Catalysis B: Environmental, 2015, 162: 98–109
46. Gonell F, Puga A V, Julián-López B, García H, Corma A. Copper-doped titania photocatalysts for simultaneous reduction of CO_2 and production of H_2 from aqueous sulfide. Applied Catalysis B: Environmental, 2016, 180: 263–270
47. Fang B, Xing Y, Bonakdarpour A, Zhang S, Wilkinson D P. Hierarchical CuO–TiO_2 hollow microspheres for highly efficient photodriven reduction of CO_2 to CH_4. ACS Sustainable Chemistry & Engineering, 2015, 3(10): 2381–2388
48. Zhai Q, Xie S, Fan W, Zhang Q, Wang Y, Deng W, Wang Y. Photocatalytic conversion of carbon dioxide with water into methane: platinum and copper(I) oxide co-catalysts with a core–shell structure. Angewandte Chemie, 2013, 125(22): 5888–5891
49. Xie S, Wang Y, Zhang Q, Deng W, Wang Y. MgO- and Pt-Promoted TiO_2 as an efficient photocatalyst for the preferential reduction of carbon dioxide in the presence of water. ACS Catalysis, 2014, 4(10): 3644–3653
50. Neațu Ș, Maciá-Agulló J A, Concepción P, Garcia H. Gold–copper nanoalloys supported on TiO_2 as photocatalysts for CO_2 reduction by water. Journal of the American Chemical Society, 2014, 136(45): 15969–15976
51. Lee S, Jeong S, Kim W D, Lee S, Lee K, Bae W K, Moon J H, Lee S, Lee D C. Low-coordinated surface atoms of CuPt alloy cocatalysts on TiO_2 for enhanced photocatalytic conversion of CO_2. Nanoscale, 2016, 8(19): 10043–10048
52. Xiong Z, Lei Z, Kuang C C, Chen X, Gong B, Zhao Y, Zhang J, Zheng C, Wu J C S. Selective photocatalytic reduction of CO_2 into CH_4 over Pt-Cu_2O TiO_2 nanocrystals: the interaction between Pt and Cu_2O cocatalysts. Applied Catalysis B: Environmental, 2017, 202: 695–703
53. Kang Q, Wang T, Li P, Liu L, Chang K, Li M, Ye J. Photocatalytic reduction of carbon dioxide by hydrous hydrazine over Au–Cu alloy nanoparticles supported on $SrTiO_3$/TiO_2 coaxial nanotube arrays. Angewandte Chemie, 2015, 127(3): 855–859
54. Farsinezhad S, Sharma H, Shankar K. Interfacial band alignment for photocatalytic charge separation in TiO_2 nanotube arrays coated with CuPt nanoparticles. Physical Chemistry Chemical Physics, 2015, 17(44): 29723–29733
55. Kar P, Farsinezhad S, Mahdi N, Zhang Y, Obuekwe U, Sharma H, Shen J, Semagina N, Shankar K. Enhanced CH_4 yield by photocatalytic CO_2 reduction using TiO_2 nanotube arrays grafted with Au, Ru, and ZnPd nanoparticles. Nano Research, 2016, 9(11):

3478–3493

56. Tan D, Zhang J, Shi J, Li S, Zhang B, Tan X, Zhang F, Liu L, Shao D, Han B. Photocatalytic CO_2 transformation to CH_4 by Ag/Pd bimetals supported on N-Doped TiO_2 nanosheet. ACS Applied Materials & Interfaces, 2018, 10(29): 24516–24522
57. Tahir B, Tahir M, Amin N S. Gold–indium modified TiO_2 nanocatalysts for photocatalytic CO_2 reduction with H_2 as reductant in a monolith photoreactor. Applied Surface Science, 2015, 338: 1–14
58. Tahir M, Amin N S. Photocatalytic CO_2 reduction with H_2 as reductant over copper and indium co-doped TiO_2 nanocatalysts in a monolith photoreactor. Applied Catalysis A, General, 2015, 493: 90–102
59. Tahir M, Amin N S. Performance analysis of nanostructured NiO–In_2O_3/TiO_2 catalyst for CO_2 photoreduction with H_2 in a monolith photoreactor. Chemical Engineering Journal, 2016, 285: 635–649
60. Tahir M, Tahir B, Saidina Amin N A, Alias H. Selective photocatalytic reduction of CO_2 by H_2O/H_2 to CH_4 and CH_3OH over Cu-promoted In_2O_3/TiO_2 nanocatalyst. Applied Surface Science, 2016, 389: 46–55
61. Pham T D, Lee B K. Novel photocatalytic activity of Cu@V co-doped TiO_2/PU for CO_2 reduction with H_2O vapor to produce solar fuels under visible light. Journal of Catalysis, 2017, 345: 87–95
62. Asahi R, Morikawa T, Irie H, Ohwaki T. Nitrogen-doped titanium dioxide as visible-light-sensitive photocatalyst: designs, developments, and prospects. Chemical Reviews, 2014, 114(19): 9824–9852
63. Akple M S, Low J, Qin Z, Wageh S, Al-Ghamdi A A, Yu J, Liu S. Nitrogen-doped TiO_2 microsheets with enhanced visible light photocatalytic activity for CO_2 reduction. Chinese Journal of Catalysis, 2015, 36(12): 2127–2134
64. Zhang Z, Huang Z, Cheng X, Wang Q, Chen Y, Dong P, Zhang X. Product selectivity of visible-light photocatalytic reduction of carbon dioxide using titanium dioxide doped by different nitrogen-sources. Applied Surface Science, 2015, 355: 45–51
65. Wang K, Yu J, Liu L, Hou L, Jin F. Hierarchical P-doped TiO_2 nanotubes array@Ti plate: towards advanced CO_2 photocatalytic reduction catalysts. Ceramics International, 2016, 42(14): 16405–16411
66. Olowoyo J O, Kumar M, Jain S L, Shen S, Zhou Z, Mao S S, Vorontsov A V, Kumar U. Reinforced photocatalytic reduction of CO_2 to fuel by efficient S-TiO_2: significance of sulfur doping. International Journal of Hydrogen Energy, 2018, 43(37): 17682–17695
67. He Z, Yu Y, Wang D, Tang J, Chen J, Song S. Photocatalytic reduction of carbon dioxide using iodine-doped titanium dioxide with high exposed {001} facets under visible light. RSC Advances, 2016, 6(28): 23134–23140
68. Tu W, Zhou Y, Liu Q, Yan S, Bao S, Wang X, Xiao M, Zou Z. An *in situ* simultaneous reduction-hydrolysis technique for fabrication of TiO_2-graphene 2D sandwich-like hybrid nanosheets: graphene-promoted selectivity of photocatalytic-driven hydrogenation and coupling of CO_2 into methane and ethane. Advanced Functional Materials, 2013, 23(14): 1743–1749
69. Wada K, Ranasinghe C S K, Kuriki R, Yamakata A, Ishitani O, Maeda K. Interfacialmanipulation by rutile TiO_2 nanoparticles to boost CO_2 reduction into CO on a metal-complex/semiconductor hybrid photocatalyst. ACS Applied Materials & Interfaces, 2017, 9(28): 23869–23877
70. Jin B, Yao G, Jin F, Hu Y H. Photocatalytic conversion of CO_2 over C_3N_4-based catalysts. Catalysis Today, 2018, 316: 149–154
71. Li H, Gao Y, Wu X, Lee P H, Shih K. Fabrication of heterostructured g-C_3N_4/Ag-TiO_2 hybrid photocatalyst with enhanced performance in photocatalytic conversion of CO_2 under simulated sunlight irradiation. Applied Surface Science, 2017, 402: 198–207
72. Dong C, Xing M, Zhang J. Double-cocatalysts promote charge separation efficiency in CO_2 photoreduction: spatial location matters. Materials Horizons, 2016, 3(6): 608–612
73. Meng X, Wang T, Liu L, Ouyang S, Li P, Hu H, Kako T, Iwai H, Tanaka A, Ye J. Photothermal conversion of CO_2 into CH_4 with H_2 over group VIII nanocatalysts: an alternative approach for solar fuel production. Angewandte Chemie International Edition, 2014, 53(43): 11478–11482